Computational Materials Science 260 (2025) 114210

Contents lists available at ScienceDirect

Computational Materials Science

journal homepage: www.elsevier.com/locate/commatsci

Full length article

Bayesian Optimization of flame-retardant performance in a high-Tg epoxy resin system

Niko Krebs [a,1], Martin Demleitner [a,1], Rodrigo Q. Albuquerque [a], Bernhard Schartel [b], Holger Ruckdäschel [a,c,*]

[a] Department of Polymer Engineering, University of Bayreuth, Universitätsstraße 30, 95447 Bayreuth, Germany
[b] Bundesanstalt für Materialforschung und -prüfung (BAM), Unter den Eichen 87, 12205 Berlin, Germany
[c] Neue Materialien Bayreuth GmbH, Gottlieb-Keim-Straße 60, 95448 Bayreuth, Germany

ARTICLE INFO

Keywords:
Machine learning
Epoxy resin
Bayesian optimization
Flame retardancy
Cone calorimeter

ABSTRACT

Polymeric materials are widely used due to their mechanical properties and cost-effectiveness, but their inherent flammability requires effective flame-retardant additives to meet safety standards. Optimizing multi-component flame-retardant formulations is challenging due to the vast experimental space. This study applies Bayesian Optimization (BO) to optimize flame-retardant formulations in high glass transition temperature (Tg) epoxy resins. Aluminum diethyl phosphinate (AlPi) was systematically combined with three synergists: zinc stannate (ZnSt), a silicone-based additive (DowSil), and low-melting glass frits (Ceepree). BO-guided experimental design expanded from 16 initial formulations to a total of 28, minimizing the Maximum Average Rate of Heat Emission (MARHE) under the constraint of Total Smoke Production (TSP) < 17 m^2 using the epsilon-constraint method. BO revealed non-linear synergistic interactions: ZnSt significantly reduced smoke production while AlPi effectively lowered heat release. The optimized formulation (BO7) achieved the lowest MARHE (122 kW/m^2) while maintaining acceptable smoke levels, establishing a new Pareto front. The results demonstrate the effectiveness of BO in accelerating the development of synergistic, halogen-free flame-retardant polymer systems, offering a scalable and sustainable approach to polymer formulation design.

1. Introduction

Polymers and polymeric composites are in high demand across various industries – such as transportation, construction, and electronics – due to their excellent specific mechanical properties, corrosion resistance, and lower cost compared to metallic counterparts. However, because of their organic nature, they are generally intrinsically flammable, making the use of flame retardants essential to enhance their fire performance and ensure compliance with required safety regulations.

Here, multicomponent flame retardant systems that rely on synergistic effects are often used to meet these requirements. For example, dripping of burning melt in the UL 94 vertical burn test is a critical failure mode for thermoplastics. Many flame-retardant polymers melt and drip when exposed to flame, which can ignite cotton placed below the specimen—disqualifying them from passing UL 94 V-0 or V-1 rating [1,2]. Here often PTFE or PFBS are additionally used in low concentrations of 0.1%–1% to prevent dripping by fibril formation as reinforcing network inside the molten polymer [3]. However Per- and polyfluoroalkyl substances including PTFE and PFBS, commonly known as PFAS are recently under increasing restrictions and there are ambitions to replace them.

For halogenated polymers, almost exclusively and well established since the 1950s, the synergist Antimony trioxide (Sb_2O_3) is used. Sb_2O_3 increases the releasing rate of halogens from aromatic halides via the formation of antimony halides and oxyhalides during combustion. They support the quenching of highly-reactive combustion radicals in the gas-phase [4,5]. Therefore, the halogen content can be significantly reduced from 15%–20% to 5%–7% with typically 1%–2% antimony trioxide [6]. However, due to a sharp ten-fold increase in the price of antimony trioxide – from $5000 in 2019 to $50,000 in 2025 – driven by Chinese export restrictions, and in light of growing regulatory pressure and environmental concerns, a clear shift toward alternative, halogen-free flame retardants is emerging.

Phosphorus- and nitrogen-based flame retardants are increasingly used – either alone or in combination – as effective replacements [7,8]. These systems work by reducing the formation of flammable volatiles

* Corresponding author at: Department of Polymer Engineering, University of Bayreuth, Universitätsstraße 30, 95447 Bayreuth, Germany.
E-mail address: holger.ruckdaeschel@uni-bayreuth.de (H. Ruckdäschel).
[1] These authors contributed equally to this work.

https://doi.org/10.1016/j.commatsci.2025.114210
Received 1 July 2025; Received in revised form 18 August 2025; Accepted 18 August 2025
Available online 16 September 2025

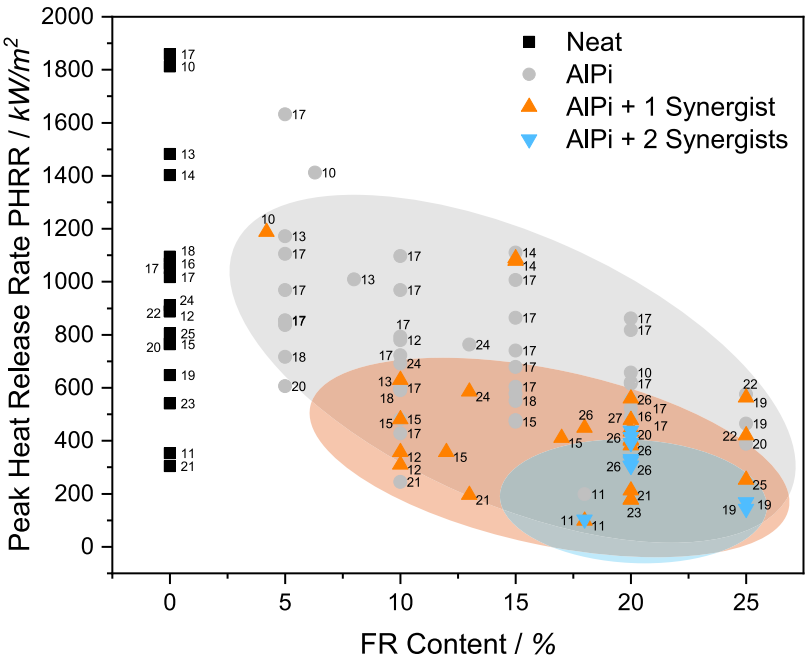

Fig. 1. Literature overview of the influence of AlPi and synergist content on the PHRR [10–27]. All measurements were carried out with 50 kW/m^2 heat flux.

and promoting the development of a dense, phosphorus-rich, crosslinked char that serves as a protective barrier for various polymers. Depending on the formulation, both combinatorial and synergistic effects on flame-retardant performance can be observed [9].

Organic phosphates and phosphinates are commercially well-established flame retardants, valued for their high phosphorus content and excellent thermal stability, which make them suitable for both thermoplastic and thermoset systems. Among these, ammonium phosphates and aluminum phosphinates (AlPi) are the most widely utilized.

Numerous studies have investigated the combinatorical/synergistic effects of various flame retardants in combination with AlPi. Fig. 1 provides an overview of the impact on the maximum heat release rate (pHRR) in different polymers, using AlPi as the primary flame retardant along with various synergists. The results reveal a clear trend: multicomponent flame retardant systems offer significantly enhanced flame retardant performance.

For instance, Goller et al. reported that the addition of 5 wt –% zinc stannate (ZnSt) as a synergist achieved a significant pHRR reduction of 30 % in polyamide 6.6 systems [28]. Furthermore, the study demonstrates the ability of ZnSt to act not only as a flame retardant enhancer but also as a smoke suppressant, thereby contributing to improved overall fire safety properties.

Similarly, the work of Sanchez-Olivarez et al. highlighted the effectiveness of incorporating 2 wt –% of *DowSil*, a silicone-based synergist, into a thermoplastic starch biocomposite system. This addition led to a remarkable pHRR reduction of 32 %, further emphasizing the role of carefully selected synergists in optimizing flame retardant efficiency in diverse polymer matrices [29].

Another promising synergist are low-melting inorganic glass frits (marketed under the brand name *Ceepree* by Azelis and *Flamtard V100* by William Blythe). As discovered by Wu et al., Ceepree forms a glassy barrier that protects the polymer from further thermal degradation, resulting in a significant reduction in pHRR of up to 63 % [30]. Recently, the combination of AlPi with Flamtard V100 in an epoxy resin and its glass-fiber-reinforced composites were explored [31,32].

However, the use of multiple flame retardants makes the optimization of flame-retardant systems challenging, as traditional trial-and-error methods and design of experiments (DoE) quickly reach their limits. For example, combining three different flame retardants at four concentration levels already results in 64 experiments, making the optimization process costly and time-consuming.

Recently, machine learning (ML) techniques have emerged as powerful tools for identifying optimal parameters and detecting correlations in large, complex datasets—without the need for explicit mathematical models [33,34]. Such approaches are particularly promising for accelerating the optimization of flame-retardant polymeric materials [35]. Recent studies often rely on large datasets – sometimes comprising several hundred data points – such as the chemical structures of flame retardants analyzed via multivariate linear regression (MLR) [36], or published cone calorimeter data used in extreme gradient boosting (XGB) models [37].

In recent years, the application of ML to materials design has expanded rapidly, enabling the efficient exploration of high-dimensional formulation spaces and the identification of structure–property relationships that are difficult to capture with conventional experimental approaches [38].

In the field of flame-retardant materials, ML has been employed to predict fire performance parameters and optimize additive combinations for enhanced flame resistance, smoke suppression, and mechanical integrity [39,40]. These methods have demonstrated the potential to accelerate the discovery of safe and effective flame-retardant formulations by guiding targeted experimentation and reducing the need for extensive trial-and-error testing.

In contrast, when working with a limited number of data points, the ML technique known as Bayesian Optimization (BO) has proven particularly effective. It significantly reduces the time required to identify optimal parameters in various polymer-related applications [41–44].

In another study, Verret et al. investigated the influence of ammonium polyphosphate (APP) and pentaerythritol (PER) on the Limiting Oxygen Index (LOI) of polypropylene. Using Multi-Objective Bayesian Optimization (MOBO), they identified an optimal total additive concentration of 24 wt. –%, comprising 17% APP and 7% PER [45]. Schenck et al. investigated the optimization of flame-retardant polyamide formulations containing up to 11 components. An initial dataset of 75 formulations was analyzed first. Subsequently, a BO approach led to a reduction in peak heat release rate (pHRR) of 73.3% compared to the neat resin, using four of the nine investigated flame retardants [46].

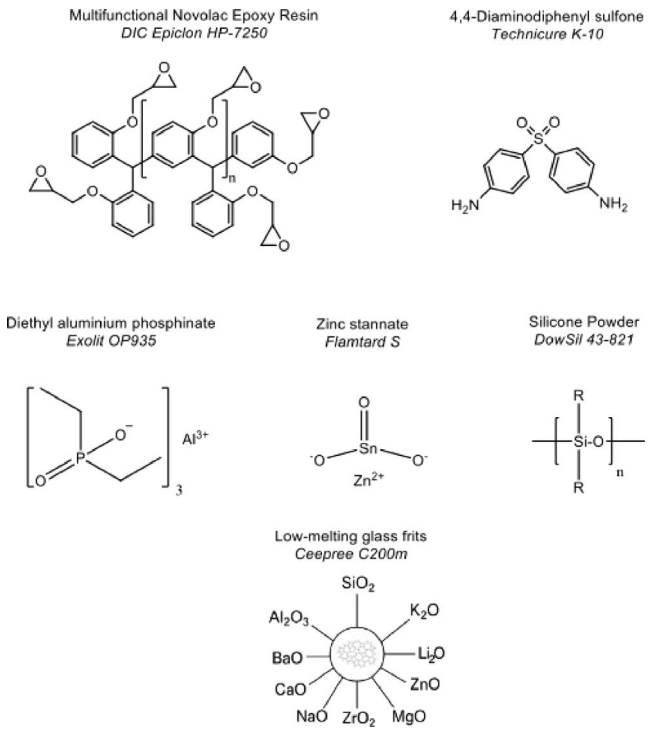

Fig. 2. Overview of the used resin system and flame retardants.

This study aims to identify an optimal AlPi-based flame retardant formulation that incorporates the three synergists: zinc stannate, DowSil, and Ceepree (CP), for a selected resin system using a BO approach [47]. Techniques such as uncertainty sampling and the ϵ-constraint method were employed to progressively improve the fire properties—peak heat release rate (PHRR) and maximum average rate of heat emission (MARHE). Here, a constrained Bayesian optimization approach was employed to minimize MARHE while keeping TSP within defined (low) limits, as both are critical factors for fire safety. The generated Pareto front serves as a visual and analytical tool to understand and quantify the trade-offs between the different objectives.

2. Experimental

2.1. Materials

The multifunctional semi-solid novolac epoxy resin Epiclon HP-7250 (DIC Corporation, Tokyo, Japan) with an epoxy equivalent weight (EEW) of 162 was used. As curing agent, micronized 4,4-diaminodiphenyl sulfone *Technicure K-10* provided by Acci Speciality Materials (Linden, NJ, USA) with a particle size of D_{50} = 10 µm was used. The amine hydrogen equivalent weight (AHEW) of the curing agent was 62.

As the primary flame retardant, diethylaluminium phosphinate *Exolit OP935* of Clariant AG (Muttenz, Switzerland) with an average particle size of D_{50} = 10 µm was used. With a high phosphorus content of 23%, good flame-retardant properties can be achieved even at low filler loading. In addition, three flame retardant synergists were incorporated: Zinc stannate *Flamtard S* provided by William Blythe (United Kingdom), low melting glass frits *Ceepree C200m* from Azelis (Belgium), and the silicone-based additive *DowSil 43-821* from Dow Chemical (USA).

Fig. 2 shows the chemical structure of the resin system and flame retardants.

2.2. Specimen preparation

The epoxy resin was preheated to 120 °C in a vacuum dissolver (VMA Getzmann Dispermat, Reichshof, Germany). Subsequently, the flame retardants were added separately, with each addition followed by at least 5 min of mixing to ensure a homogeneous dispersion. After the final flame retardant was added and thoroughly mixed, the curing agent 4,4'-DDS was introduced and mixed under continuous degassing until a uniform mixture was achieved.

The formulation was then poured into preheated vertical molds (3 mm thickness) at 120 °C. The curing cycle was carried out in a convection oven (Memmert ULE 400) and consisted of the following steps: 1 h at 120 °C, 3 h at 180 °C, and a post-curing step of 2 h at 250 °C, all with a heating rate of 3 K/min. Cooling to room temperature was performed over 12 h at a cooling rate of 1 K/min.

2.2.1. Cone calorimetric measurements

Fire testing was carried out on an iCone calorimeter from Fire Testing Technology Ltd. (East Grinstead, England). According to DIN ISO 5660, samples measuring 100 mm × 100 mm with 3 mm thickness are wrapped in an aluminum foil pocket and placed in a metal frame sample holder, which exposed 88.4 cm^2 of the sample surface. The samples were irradiated at a distance of 25 mm with a heat flux of 35 kW/m^2. Key fire behavior parameters, including the total smoke production (TSP), heat release rate (HRR), and average rate of heat emission (ARHE), were recorded to assess the flame retardancy effects. The maximum value of ARHE over the duration of the test, referred to as the MARHE, was used as one of the optimization targets in this study. To ensure reliable results, at least three samples were measured for each mixture under identical conditions. In cases where notable data variability was observed, additional replicates were considered to enhance the accuracy of the reported values.

2.3. Bayesian optimization of formulations

New formulations were proposed through iterative rounds of BO. The general procedure of Bayesian Optimization can be described as follows: First, the objective function to be optimized is defined. A surrogate model is then selected – in this case, a Gaussian Process Regressor (GPR) – to approximate the unknown objective function in a probabilistic manner. GPRs are well suited for this task due to their ability to model complex relationships, quantify prediction uncertainty, and provide interpretable outputs.

The GPR predicts the target property of a new formulation based on its similarity to previously tested samples. This similarity is quantified using a kernel function; in this work, a radial basis function (RBF) kernel was employed. The underlying assumption is that similar input features will yield similar target properties.

In addition to predicting a mean value, the GPR provides an estimate of the uncertainty associated with each prediction. This information is used in the so-called acquisition function, which evaluates a large number of virtual samples by combining their predicted means and uncertainties. The sample with the highest expected utility is selected as the next candidate for experimental validation. Depending on whether the predicted value or its uncertainty is prioritized, the algorithm performs either exploitation or exploration.

In this study, the Expected Improvement (EI) acquisition function was applied:

$$EI(\mathbf{x}) = \begin{cases} (\mu(\mathbf{x}) - f(\mathbf{x}^+) - \xi) \cdot \Phi(Z) + \sigma(\mathbf{x}) \cdot \phi(Z), \\ \quad \text{if } \sigma(\mathbf{x}) > 0 \\ 0, \quad \text{otherwise} \end{cases} \tag{1}$$

where

$$Z = \frac{\mu(\mathbf{x}) - f(\mathbf{x}^+) - \xi}{\sigma(\mathbf{x})} \tag{2}$$

Table 1
Overview of initial dataset formulations with flame retardant additives.

ID	AlPi wt.%	ZnSt wt.%	DowSil wt.%	Ceepree wt.%	Source
A0	0.00	0.00	0.00	0.00	This work
A1	5.00	0.00	0.00	0.00	This work
A2	10.00	0.00	0.00	0.00	This work
A3	20.00	0.00	0.00	0.00	This work
A4	25.00	0.00	0.00	0.00	This work
A5	0.00	0.00	0.00	15.00	This work
L1	10.00	6.50	0.00	0.00	[28]
L2	10.00	0.00	2.00	0.00	[29]
L3	10.00	0.00	0.00	2.00	[49]
L4	10.00	0.00	0.00	10.00	[30]
R1	10.90	2.58	1.28	0.00	This work
R2	6.10	6.85	2.52	0.00	This work
R3	8.74	8.28	1.13	0.00	This work
R4	11.39	7.15	3.56	0.00	This work
R5	11.56	3.24	2.28	1.81	This work
R6	9.48	1.33	1.10	2.14	This work

Here, $\mu(\mathbf{x})$ is the predicted mean and $\sigma(\mathbf{x})$ the predicted standard deviation at input $\mathbf{x}$. $f(\mathbf{x}^+)$ is the best observed function value so far, and ξ is a parameter controlling the trade-off between exploration and exploitation (set to 0.02 in this work). $\Phi(Z)$ and $\phi(Z)$ denote the cumulative distribution and probability density functions of the standard normal distribution, respectively.

The GPR hyperparameters and the EI acquisition function parameter $\xi = 0.02$ were selected based on their proven effectiveness in closely related multi-objective optimization studies on epoxy resin systems [48]. These settings have consistently yielded a balanced trade-off between exploration and exploitation and demonstrated stable convergence without requiring dedicated hyperparameter tuning. In this study, no additional hyperparameter optimization was performed, as the primary objective was to evaluate the feasibility and efficiency of BO in guiding flame-retardant formulation development under constrained experimental budgets. The use of pre-validated parameters ensured comparability with prior results and minimized the risk of overfitting to the limited dataset.

Based on prior experience with formulation optimization tasks [41, 42], the Expected Improvement function proved particularly effective.

2.3.1. Data preparation

Initial dataset. Before optimizing the target parameters MARHE and TSP, an initial dataset was generated to serve as the foundation for regression-based modeling of material behavior. This dataset includes various formulations to ensure a diverse and well-balanced representation of material compositions.

The first set of formulations consists of the base resin-hardener system and its mixtures with systematically varying the AlPi concentration to study its sole influence on flame retarding performance. The neat resin (A0) showed a MARHE of 236 kW/m^2 and a TSP of 16 m^2, serving as the baseline for comparison with all other formulations. Additionally, four flame-retardant combinations inspired by literature were incorporated to further expand the dataset. Due to limited available data on Ceepree-AlPi interactions, a formulation containing 15 wt.% Ceepree was also included.

To further enhance diversity and minimize potential bias, six additional compositions were randomly selected from the virtual dataset (explained in the next section).

Table 1 summarizes the complete list of realized formulations as part of the initial dataset, categorizing samples based on their type (AlPi-based A_n, literature-derived L_n, or randomly selected samples R_n).

Table 2
Compositional constraints for the virtual dataset.

Component	Range (wt.%)
AlPi	0–20
ZnSt	0–10
DowSil	0–10
Ceepree	0–15
Total Additives	≤ 25

2.3.2. Virtual dataset and boundary conditions

To ensure a comprehensive exploration of the formulation space, a virtual dataset was created, comprising 10^6 unique compositions. This large dataset allows for a more extensive parameter space investigation and provides an initial foundation for the Bayesian Optimization process.

The compositional constraints defining the virtual dataset were carefully chosen to balance fire performance, processability, and material feasibility. The constraints are summarized in Table 2.

2.3.3. Optimization procedure

The Bayesian Optimization process was used to iteratively refine and enhance the predictive precision of the regression model. A flowchart summarizing the optimization workflow is presented in Fig. 3, illustrating the stepwise approach used to navigate the formulation space.

2.3.4. Pareto front analysis and sample domination

A Pareto front analysis was performed to balance the optimization of MARHE and TSP. The Pareto front represents the set of formulations that achieve an optimal trade-off between these two target properties.

A formulation is considered dominant over another if it has:

- **Lower MARHE** (better fire performance)
- **Lower TSP** (less smoke production)

If a formulation F_1 has both lower MARHE and lower TSP than another formulation F_2, then F_1 dominates F_2 and is part of the pareto front. This concept is illustrated in Fig. 5, which visually maps the trade-offs between formulations.

2.3.5. Reference model and weight coefficients

To benchmark the BO-driven regression models, a simple linear reference model was established. The model follows:

$$f = \sum w_i x_i + N$$

where w_i represents the weight coefficient of each flame retardant component x_i and N describes the resin behavior without flame retardant additivation. These coefficients, derived from regression analysis, provide insights into the influence of each additive:

- **Negative coefficients** indicate performance improvement.
- **Positive coefficients** suggest a detrimental effect on MARHE or TSP.

By comparing these coefficients with the BO-driven model, the contribution of each additive can be evaluated, guiding future formulation design.

These regression-based insights into individual flame retardant contributions complement the broader goal of identifying optimal multi-component formulations. To efficiently search the vast formulation space and systematically improve fire performance, BO was employed.

BO uses a data-driven, iterative strategy that balances exploration of new material combinations with the refinement of already promising regions. The optimization loop—illustrated in Fig. 3—starts with the

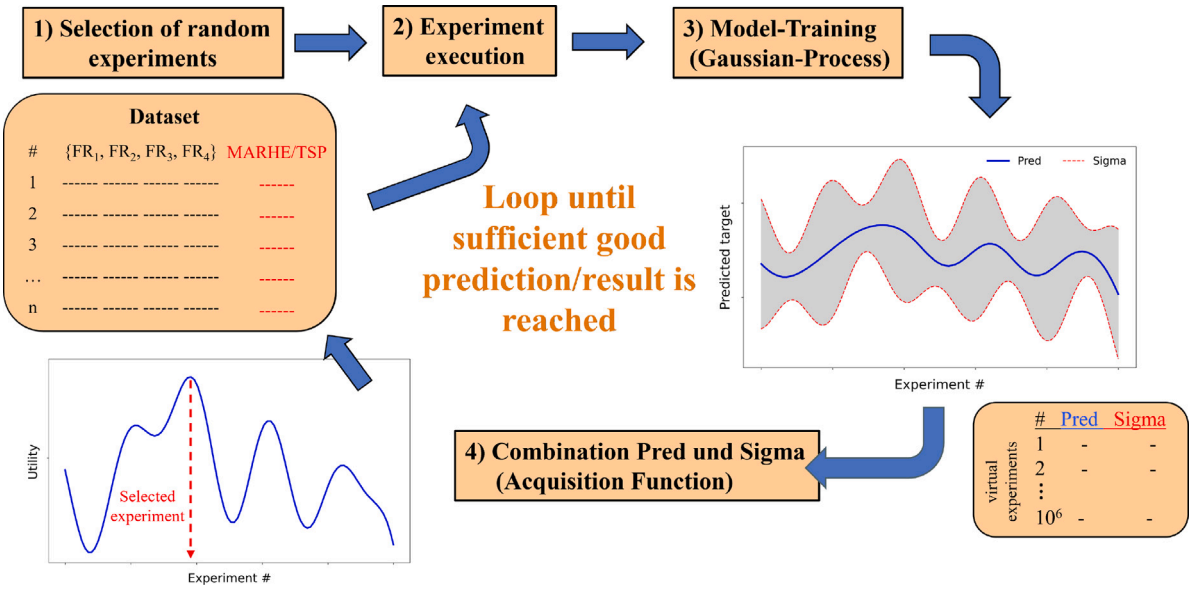

Fig. 3. Flowchart of used Bayesian optimization cycle.

selection of initial random formulations and their experimental validation. This data is then used to train a Gaussian Process (GP) model, which not only predicts MARHE and TSP for all virtual formulations, but also quantifies the uncertainty of each prediction.

The predicted values and associated uncertainties are combined using an acquisition function—specifically, the maximum expected improvement (maxEI). This guides the selection of the next most informative formulation to test. By iteratively repeating this process, the algorithm steers the search toward compositions with increasingly favorable properties while simultaneously improving its predictive accuracy.

The workflow diagram in Fig. 3 highlights this closed-loop structure, where experimentation and prediction continuously inform one another. This combination of machine learning and targeted experimentation proved to be highly effective for navigating the complex, multi-objective formulation space.

The optimization process consisted of a total of eight experimental iterations, including five BO cycles and three intermediate uncertainty sampling steps. The number of cycles was determined by practical constraints such as available material quantities, experimental time, and budget. The procedure was concluded when improvements between consecutive BO cycles became marginal and the Pareto front did not show any further significant advancement.

3. Results and discussion

Upon completion of the base dataset, the Gaussian Process regression model was applied to estimate MARHE and TSP values, along with associated prediction uncertainties, for all 10^6 virtual flame-retardant formulations.

3.1. Reduction of model uncertainty via uncertainty sampling

Given the limited initial dataset, the GP regression model exhibited high prediction uncertainty (i.e., high variance), particularly for formulations distinct from previously measured samples. To address this, uncertainty sampling was applied by selecting two compositions – one for MARHE and one for TSP – with the highest predicted variance in the Gaussian Process model.

A complete overview of all tested formulations, including their compositions as well as the measured MARHE, TSP, and PHRR values, is provided in Table S1 of the Supporting Information.

Table 3
Samples suggested by BO of MARHE/TSP.

ID	AlPi wt.%	ZnSt wt.%	DowSil wt.%	Ceepree wt.%	MARHE kW/m²	TSP m²
BO1	6.85	0.07	9.99	0.02	164	19
BO2	5.96	0.11	9.83	8.95	163	17
BO3	19.85	4.57	0.07	0.03	128	16
BO4	6.16	8.71	0.15	9.91	153	13
US3	6.10	2.30	5.10	0.80	160	18

US1 and US2 both featured low AlPi content combined with high proportions of ZnSt and Ceepree—combinations not yet represented in the existing dataset. Additionally, US1 included 4.4 wt.% DowSil, thereby covering a previously unexplored three-component region within the formulation space.

Although these samples were not intended for performance optimization, the cone calorimeter measurements revealed consistent fire behavior. US2 achieved a slightly lower MARHE than US1 (reduced by approximately 11%), with both samples showing identical TSP values. Importantly, US2 was located on the fourth Pareto front, indicating a previously unreached balanced trade-off between MARHE and TSP. This highlights the effectiveness of uncertainty sampling in identifying unexplored yet promising regions of the formulation space.

These findings underscore the importance of targeted data acquisition in underrepresented composition ranges to improve model robustness and support efficient optimization in subsequent iterations.

3.2. Target property optimization of MARHE and TSP by Bayesian optimization

Following the incorporation of uncertainty sampling, the first BO round was conducted to improve the fire performance metrics MARHE and TSP. Based on the augmented dataset, two formulations were proposed—each optimized individually for one of the two target properties (Table 3).

BO1 aimed to minimize MARHE and comprised 6.9 wt.% AlPi and the maximum allowed 10.0 wt.% DowSil.

BO2, optimized for TSP, included similar AlPi content (6.2 wt.%) but had a substantially increased Ceepree content (from 0.02 wt.% in BO1 to 8.95 wt.%), while maintaining a similar DowSil level.

The ZnSt content remained negligible in both cases.

Table 4
Samples suggested by Bayesian optimization of MARHE under TSP constraint.

ID	AlPi wt.%	ZnSt wt.%	DowSil wt.%	Ceepree wt.%	MARHE kW/m²	TSP m²
BO5	19.83	0.06	0.12	4.90	131	18
BO6	17.07	0.09	7.60	0.12	239	13

Cone calorimeter results showed that neither sample significantly outperformed the existing data. MARHE values were nearly identical for both BO1 and BO2, and TSP values showed only a slight improvement in BO2. Consequently, neither formulation qualified for inclusion in the updated Pareto front.

To enhance model robustness, a third composition was additionally selected via uncertainty sampling. The new BO suggestions – targeting MARHE and TSP, respectively – featured almost no DowSil, indicating that its contribution to performance in this system is limited.

The MARHE-optimized sample from this round contained 19.9 wt.% AlPi and 4.6 wt.% ZnSt, while the Ceepree content was reduced to a very small level. This observation aligns with previous findings suggesting a positive correlation between high AlPi content and reduced MARHE. In contrast, the TSP-optimized sample combined moderate AlPi content (6.2 wt.%) with 9.9 wt.% Ceepree and 8.7 wt.% ZnSt—aligning with literature reports on the smoke-suppressing effects of ZnSt.

Cone calorimetry confirmed this differentiation: the MARHE-optimized sample achieved the second-lowest MARHE value thus far (128 kW/m²), while the TSP-optimized sample recorded a relatively low TSP of 13 m². The uncertainty sampling point did not contribute to further improvement in either property but enhanced coverage of the formulation space.

These results confirm the value of Bayesian optimization for iterative formulation improvement and demonstrate the importance of balancing exploration and exploitation to guide experimental design.

3.3. Bayesian optimization of MARHE under TSP constraint

To simultaneously fulfill the regulatory limits for MARHE and TSP, the optimization strategy was adapted using the epsilon-constraint method. Based on the shape of the current Pareto front—resembling a hyperbolic trade-off it was concluded that MARHE remained the more critical property to be improved. Consequently, MARHE was selected as the primary optimization target, while TSP was constrained to remain below 17 m². This approach ensures that newly suggested formulations are located within the desired target region of the result space, characterized by simultaneously low MARHE and TSP values.

This constraint was applied to the entire virtual dataset by filtering out all compositions with predicted TSP values above this threshold. The resulting filtered dataset contained approximately 396 000 samples, serving as the new search space (virtual dataset) for subsequent BO rounds.

Two additional BO cycles were performed using this filtered dataset (Table 4). Both BO5 and BO6 suggested high AlPi contents—19.8 wt.% and 17.1 wt.%, respectively—confirming the established correlation between AlPi loading and MARHE reduction. ZnSt was nearly absent in both formulations, while Ceepree and DowSil were each explored once as the sole synergist. The flame retardant ratios of AlPi to synergist varied between 4.0 and 2.2, allowing targeted comparison of their effects.

Experimental results revealed that BO5 reached a MARHE of 131 kW/m², close to the best values achieved so far. However, its TSP of 18 m² exceeded the defined constraint and disqualified the formulation from the updated Pareto front. BO6, which relied on DowSil as synergist, resulted in a substantially higher MARHE of 239 kW/m², suggesting that DowSil does not contribute effectively to MARHE reduction in this system. Its TSP value of 13 m² did meet the constraint.

Table 5
Included samples from scientific intuition and final BO round.

ID	AlPi wt.%	ZnSt wt.%	DowSil wt.%	Ceepree wt.%	MARHE kW/m²	TSP m²
SI1	0.00	10.00	0.00	0.00	202	12
SI2	5.00	10.00	0.00	0.00	165	11
BO7	15.28	8.98	0.00	0.00	122	16

Neither BO5 nor BO6 qualified for the updated Pareto front, indicating that while the epsilon-constraint approach effectively focused the virtual dataset, further refinement of the data would be required for continued progress.

3.4. Incorporation of scientific intuition to improve the BO model

Recent BO iterations revealed a stagnation in performance gains, suggesting that further progress would require refinement of the dataset itself. To support this, results from earlier cycles were revisited, particularly the effective MARHE reduction observed in sample BO3, which combined AlPi with ZnSt. This prompted a hypothesis-driven investigation into the specific effect of ZnSt as a synergist.

To test this, two new samples were designed and experimentally validated (Table 5). SI1 contained 10 wt.% ZnSt as the sole flame retardant, while SI2 combined 10 wt.% ZnSt with 5 wt.% AlPi—resulting in an AlPi:ZnSt ratio of 0.5, identical to that in BO3. These compositions aimed to isolate and clarify the synergistic potential of ZnSt, especially in low-AlPi systems.

The results confirmed that ZnSt effectively suppresses smoke formation. SI1 achieved a TSP of 12 m², which is significantly below average, despite containing only 10 wt.% total flame retardant. However, its MARHE was comparable to the neat sample, indicating limited effect on heat release. SI2, on the other hand, exhibited a further reduction in TSP to 11 m² and a substantial MARHE improvement to 165 kW/m². This confirmed the beneficial interaction between AlPi and ZnSt.

Guided by this insight, a subsequent BO cycle was executed using the epsilon-constraint method (Table 5). The newly suggested sample, BO7, combined AlPi and ZnSt and resulted in a MARHE of 122 kW/m²—the lowest value recorded in the entire study. Additionally, it was the first formulation to reduce the peak heat release below 200 kW/m².

This demonstrates that integrating targeted experimental knowledge into the optimization workflow can enhance the efficiency and accuracy of the BO model. BO7 defines the new optimal formulation on the final Pareto front, dominating all previous candidates in MARHE while maintaining acceptable TSP performance.

3.5. Overview of the stepwise optimization progress

The success of the BO strategy is illustrated by tracking the normalized MARHE and TSP values across all experimental iterations Fig. 4. The values are normalized with respect to the neat reference formulation, enabling a direct comparison of flame-retardant performance. While early samples – including random and literature-based formulations – showed limited improvement, a clear downward trend in both metrics emerges following the introduction of BO-guided suggestions. This reflects the increasing effectiveness of targeted exploration and model refinement throughout the optimization process.

The evolution of the Pareto front is shown in Fig. 5, highlighting the shift in optimal trade-offs between MARHE and TSP across different BO cycles. As new, data-driven formulations were introduced, the Pareto front progressively moved toward the lower left region of the result space—indicating simultaneous improvement in both objectives. The final front includes BO7, which defines the lowest MARHE value in the dataset while maintaining acceptable TSP performance.

Together, these visualizations underscore the efficiency of the BO workflow in systematically guiding the experimental design toward the constrained optimization of MARHE under a TSP bound.

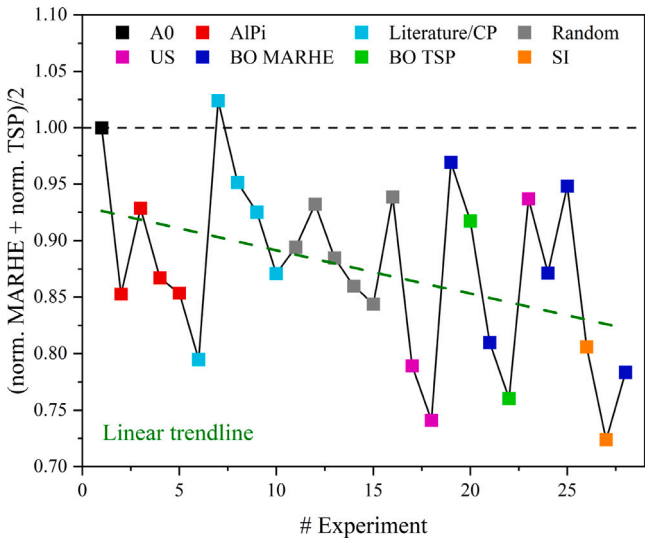

Fig. 4. Normalized development of MARHE and TSP in course of the optimization. The dashed dark green line shows the linear trend during optimization.

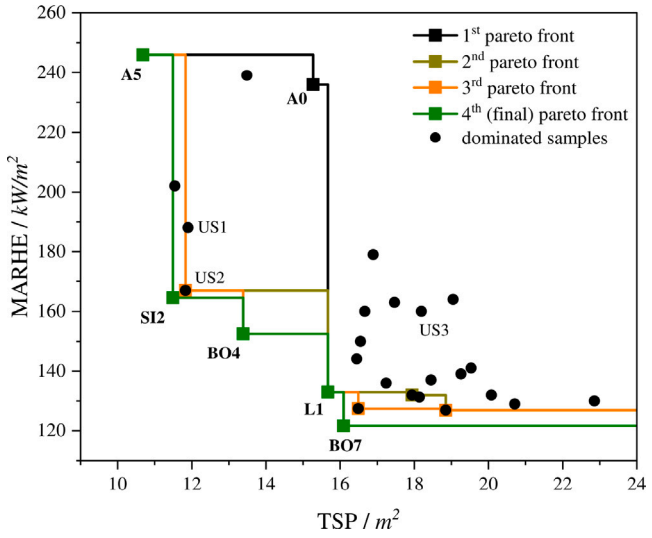

Fig. 5. Evolution of the Pareto front in the MARHE–TSP objective space. Each color represents a different stage of the optimization process. Black dots indicate dominated samples not part of the Pareto front.

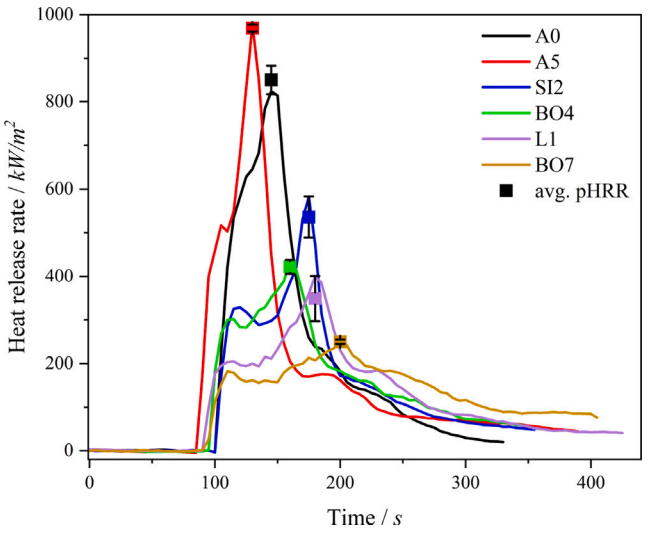

Fig. 6. Development of the HRR for the Pareto samples.

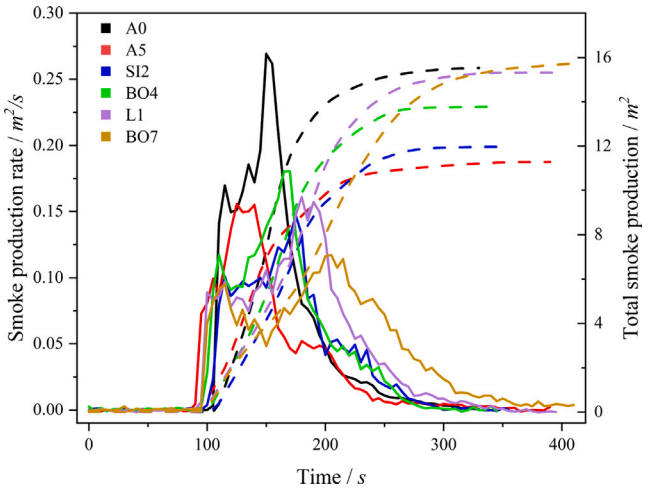

Fig. 7. Smoke behavior of all Pareto samples.

3.6. Detailed fire behavior analysis of selected formulations

To deepen the understanding of flame-retardant mechanisms beyond aggregated performance values, selected formulations from the Pareto front were analyzed in detail using further data from cone calorimetric analysis. The temporal profiles of heat release and smoke production provide insight into the interplay between the applied flame retardants.

Optimized formulations – especially BO7, containing AlPi, ZnSt, and CP – show a delayed and flattened fire development. This is evident in the heat release rate (HRR) profile (Fig. 6), which demonstrates significantly reduced peak intensities and a prolonged growth phase. Such behavior indicates efficient flame inhibition and increased thermal stability under fire conditions.

While AlPi effectively lowers MARHE, it tends to increase TSP. ZnSt, in contrast, has a pronounced smoke-suppressing effect. CP complements this by acting as a barrier former, further reducing the heat release. The combined effect of ZnSt and CP results in lower TSP without compromising heat emission behavior, as visualized in the TSP and smoke production rate (SPR) curves (Fig. 7).

For instance, BO7 achieved a MARHE of 122 kW/m^2 and a TSP of 16 m^2, balancing both performance metrics within acceptable limits. These observations confirm the value of synergistic multi-component systems: AlPi governs heat release, ZnSt suppresses smoke, and Ceepree enhances residue formation. Their combined use allows for improved efficiency at lower total loadings, supporting processability and material integrity in application-specific formulations. To gain deeper insight into the underlying flame-retardant mechanisms, selected formulations were examined after combustion, focusing on the morphology of the resulting char residues. A comparison of representative samples revealed three distinct types of char formation, each associated with different fire performance profiles.

In the neat resin (A0), combustion left behind only a fragmented and porous residue without any coherent protective layer, with a residue yield of 33%. This insufficient barrier formation is directly reflected in high MARHE values and average TSP results, highlighting the limited intrinsic flame resistance of the base resin. In contrast, US1, a CP-rich formulation with low AlPi content, formed a dense and stable char layer with a smooth and unbroken surface, corresponding to a residue yield of 49%. This melt-derived barrier remained mechanically intact after combustion and effectively suppressed smoke evolution.

(a) (b) (c)

Fig. 8. Residual char layer of sample A0 (a), US1 (b) and BO7 (c) after cone measurement.

Table 6
Linear regression coefficients for the influence of each flame retardant on MARHE and TSP.

FR	MARHE	TSP
AlPi	−188	+7
ZnSt	−36	−17
DowSil	+71	0
CP	+29	−9
k_0	159	16

A third and particularly effective type of residue was observed in BO7, which combines AlPi and ZnSt. This formulation produced a voluminous, intumescent char that expanded during combustion, with a residue yield of 50%. The resulting structure provided strong insulation and radical quenching effects, leading to the lowest MARHE values observed in the study.

A visual impression of the degraded residues is shown in Fig. 8.

These observations demonstrate that the type and quality of char formation critically determine the balance between heat release suppression and smoke development. A stable and continuous barrier promotes low smoke generation, while intumescence enhances thermal shielding but may compromise smoke performance.

4. Linear regression analysis

To assess the influence of individual flame retardants on the key fire performance parameters, a multiple linear regression (MLR) was applied to the whole dataset. The goal of this simplified model was not to predict target properties with high accuracy, but rather to extract general trends and directionality in the influence of each component.

The regression follows the general form:

$$y = k_0 + k_{\mathrm{AlPi}} \cdot x_{\mathrm{AlPi}} + k_{\mathrm{ZnSt}} \cdot x_{\mathrm{ZnSt}} + k_{\mathrm{DowSil}} \cdot x_{\mathrm{DowSil}} + k_{\mathrm{CP}} \cdot x_{\mathrm{CP}} \quad (3)$$

where y is the target property (either MARHE or TSP), x_i is the mass fraction of flame retardant i, and k_i are the corresponding regression coefficients. The intercept k_0 represents the baseline property of the material without any flame retardant (i.e., formulation A0). Prior to regression, all input variables were standardized using a z-score transformation (StandardScaler) to ensure comparability of coefficients and to eliminate scale bias.

The resulting regression coefficients for MARHE and TSP are summarized in Table 6. Negative values indicate a reducing effect on the respective target value, whereas positive values correspond to an increase.

Detailed regression plots for MARHE and TSP are provided in the Supporting Information as Figs. S1 and S2, respectively.

The results confirm several trends already observed during the optimization. AlPi and ZnSt both contributed to a reduction in MARHE, with AlPi having the strongest impact. However, AlPi also increased TSP, in contrast to ZnSt, which showed the most significant smoke-suppressing effect. CP and DowSil were found to influence MARHE negatively in the linear model, indicating that they are not suitable for use as flame retardants in this resin system to reduce MARHE.

The suitability of the linear regression was evaluated by comparing predicted and measured values. The respective correlation plots for MARHE and TSP are provided as Supporting Figures. While the general trends are captured, the scatter in the plots illustrates the limitations of a purely linear model, especially for compositions with strong synergistic behavior.

This analysis supports the interpretation of the BO results and provides a straightforward summary of how each flame retardant contributes to heat release and smoke production in isolation.

5. Conclusion

This study successfully demonstrates the application of Bayesian Optimization as an efficient and data-driven methodology to enhance flame-retardant performance in high-T_g epoxy resin systems. By integrating machine learning with targeted experimental validation, the multicomponent optimization of aluminum diethyl phosphinate (AlPi) in combination with synergists – zinc stannate (ZnSt), a silicone-based additive (DowSil), and a low-melting glass frit (Ceepree) – was achieved in a resource-efficient manner.

The BO workflow enabled the identification of complex, non-linear, and synergistic effects between the additives, which would be difficult to uncover via traditional trial-and-error approaches. Notably, ZnSt emerged as a key synergist for smoke suppression, while AlPi remained the principal agent for reducing heat release. The optimized formulation BO7, combining AlPi and ZnSt, delivered the lowest recorded MARHE (122 $\mathrm{kW/m^2}$) and simultaneously fulfilled smoke production constraints, defining a new Pareto-optimal front.

This research highlights the potential of Bayesian Optimization not only as a powerful tool for flame-retardant formulation development but also as a broadly applicable strategy for accelerating the design of high-performance, halogen-free, and sustainable polymer systems.

CRediT authorship contribution statement

Niko Krebs: Writing – original draft, Methodology, Investigation, Formal analysis, Data curation. **Martin Demleitner:** Writing – review & editing, Writing – original draft, Validation, Investigation, Formal analysis, Data curation, Conceptualization. **Rodrigo Q. Albuquerque:** Writing – review & editing, Validation, Supervision. **Bernhard Schartel:** Writing – review & editing, Conceptualization. **Holger Ruckdäschel:** Writing – review & editing, Conceptualization.

Declaration of competing interest

The authors declare that they have no known competing financial interests or personal relationships that could have appeared to influence the work reported in this paper.

Acknowledgments

The authors are grateful toward Florian Puchtler of the Chair of Inorganic Chemistry I at the University of Bayreuth for the introduction and support in the Cone calorimeter measurements.

Appendix A. Supplementary data

Supplementary material related to this article can be found online at https://doi.org/10.1016/j.commatsci.2025.114210.

Data availability

Data will be made available on request.

References

[1] Y. Wang, J. Jow, K. Su, J. Zhang, Dripping behavior of burning polymers under UL94 vertical test conditions, J. Fire Sci. 30 (2012) 477–501.

[2] M. Matzen, B. Kandola, C. Huth, B. Schartel, Influence of flame retardants on the melt dripping behaviour of thermoplastic polymers, Materials 8 (2015) 5621–5646.

[3] H. Nishihara, S. Tanh, High-order structure and flame retardation effect of poly(tetrafluoroethylene) in thermoplastic resin compositions, Polym. J. 30 (1998) 322–326.

[4] V.I. Babushok, P. Deglmann, R. Krämer, G.T. Linteris, Influence of antimony-halogen additives on flame propagation, Combust. Sci. Technol. 189 (2017) 290–311.

[5] J. Simon, T. Kántor, T. Kozma, E. Pungor, Thermal analysis of Sb2O3/organohalide-based flame retardants including atomic absorption detection of the evolved species, J. Therm. Anal. 25 (1982) 57–77.

[6] A.B. Morgan, C.A. Wilkie, Fire retardancy of polymeric materials, Fire Retard. Polym. Mater. (2024) 1–775.

[7] S. Levchik, C.A. Wilkie, Char formation, Fire Retard. Polym. Mater. 589 (2000).

[8] H. Cheng, J. Guo, Y. Ye, T. Zhao, J. Cui, B. Yang, B. Mu, L. Tian, X. Bao, X. Zhang, Y. Zhou, Molecular design and properties of intrinsic flame-retardant P-N synergistic epoxy resin, J. Appl. Polym. Sci. 141 (2024) e54885.

[9] B. Schartel, Phosphorus-based flame retardancy mechanisms—Old hat or a starting point for future development? Materials 3 (2010) 4710–4745.

[10] T. Köppl, S. Brehme, F. Wolff-Fabris, V. Altstädt, B. Schartel, M. Döring, Structure-property relationships of halogen-free flame-retarded poly(butylene terephthalate) and glass fiber reinforced PBT, J. Appl. Polym. Sci. 124 (2012) 9–18.

[11] U. Braun, B. Schartel, M.A. Fichera, C. Jäger, Flame retardancy mechanisms of aluminium phosphinate in combination with melamine polyphosphate and zinc borate in glass-fibre reinforced polyamide 6,6, Polym. Degrad. Stab. 92 (2007) 1528–1545.

[12] H. Feng, D. Li, B. Cheng, T. Song, R. Yang, A cross-linked charring strategy for mitigating the hazards of smoke and heat of aluminum diethylphosphonate/polyamide 6 by caged octaphenyl polyhedral oligomeric silsesquioxanes, J. Hazard. Mater. 424 (2022) 127420.

[13] E. Gallo, B. Schartel, U. Braun, P. Russo, D. Acierno, Fire retardant synergisms between nanometric Fe2/O3 and aluminum phosphinate in poly(butylene terephthalate), Polym. Adv. Technol. 22 (2011) 2382–2391.

[14] F. Hao, Y. Chen, Z. Sun, L. Qian, Component ratio effects of melamine cyanurate and aluminum diethylphosphinate in flame retardant TPU, J. Polym. Res. 30 (2023) 25.

[15] G. Sanchez-Olivares, S. Rabe, R. Pérez-Chávez, F. Calderas, B. Schartel, Industrial-waste agave fibres in flame-retarded thermoplastic starch biocomposites, Compos. B Eng. 177 (2019) 107370.

[16] P. Müller, B. Schartel, Melamine poly(metal phosphates) as flame retardant in epoxy resin: Performance, modes of action, and synergy, J. Appl. Polym. Sci. 133 (2016).

[17] S. Rabe, Y. Chuenban, B. Schartel, Exploring the modes of action of phosphorus-based flame retardants in polymeric systems, Materials 10 (2017) 455.

[18] M. Friedel, J.V. Boehm, H. Ruckdaeschel, Impact of aluminum diethyl phosphinate (DEPAL) flame retardant on the thermal, mechanical, and fire-resistance properties of an amine-cured epoxy resin, J. Appl. Polym. Sci. 142 (2025) e56923.

[19] F. Tomiak, A. Schoeffel, K. Rathberger, D. Drummer, A synergistic flame retardant system based on expandable graphite, aluminum (diethyl-)polyphospinate and melamine polyphosphate for polyamide 6, Polymers 13 (2021) 2712.

[20] Y. Wang, D. Jiang, X. Wen, T. Tang, K. Szymańska, K. Sielicki, K. Wenelska, E. Mijowska, Investigating the effect of aluminum diethylphosphinate on thermal stability, flame retardancy, and mechanical properties of poly(butylene succinate), Front. Mater. 8 (2021).

[21] R. Zhou, W. Li, J. Mu, Y. Ding, J. Jiang, Synergistic effects of aluminum diethylphosphinate and melamine on improving the flame retardancy of phenolic resin, Materials 13 (2019) 158.

[22] Y. Ren, D. Tang, Y. Liu, Q. Wang, Enhanced flame retardancy in PA12 composites via the synergy of aluminum diethylphosphonate and melamine polyphosphate, J. Appl. Polym. Sci. (2025) e57270.

[23] Y. Lu, J. Feng, D. Yi, H. Xie, Z. Xu, C.F. Cao, S. Huo, H. Wang, P. Song, Strong synergistic effects between P/N-containing supramolecular microplates and aluminum diethylphosphinate for fire-retardant PA6, Compos. A Appl. Sci. Manuf. 176 (2024) 107834.

[24] Z. Liu, B. Huang, M. Ma, S. Chen, Y. Shi, H. He, Y. Zhu, X. Wang, Strong synergistic effects between boron-containing compounds and aluminum diethylphosphinate for enhanced fire safety and mechanical properties of polyamide 6, ACS Appl. Polym. Mater. (2024).

[25] J. Reuter, L. Greiner, P. Kukla, M. Döring, Efficient flame retardant interplay of unsaturated polyester resin formulations based on ammonium polyphosphate, Polym. Degrad. Stab. 178 (2020) 109134.

[26] A. Bachinger, A. Sandinge, K.M. Lindqvist, A. Strid, G. Gong, Systematic evaluation of bromine-free flame-retardant systems in <scp>acrylonitrile-butadiene-styrene</scp>, J. Appl. Polym. Sci. 139 (2022).

[27] A. Sut, S. Greiser, C. Jäger, B. Schartel, Synergy in flame-retarded epoxy resin, J. Therm. Anal. Calorim. 128 (2017) 141–153.

[28] S.M. Goller, S. Krüger, B. Schartel, No business as usual: The effect of smoke suppressants commonly used in the flame retardant PA6.6 on smoke and fire properties, Polym. Degrad. Stab. 209 (2023) 110276.

[29] G. Sanchez-Olivares, S. Rabe, R. Pérez-Chávez, F. Calderas, B. Schartel, Industrial-waste agave fibres in flame-retarded thermoplastic starch biocomposites, Compos. B Eng. 177 (2019) 107370.

[30] G.M. Wu, B. Schartel, M. Kleemeier, A. Hartwig, Flammability of layered silicate epoxy nanocomposites combined with low-melting inorganic ceepree glass, Polym. Eng. Sci. 52 (2012) 507–517.

[31] M. Jauregui Rozo, S. Sunder, W. Tabaka, B. Klaffke, H. Ruckdäschel, B. Schartel, Unveiling aluminum diethyl phosphinate dual identity: Transfer from epoxy resins to glass fiber-reinforced composites, Polym. Compos. (2025).

[32] S. Sunder, M. Jauregui Rozo, S. Inasu, D. Meinel, B. Schartel, H. Ruckdäschel, Effect of ammonium polyphosphate/silicate content on the postfire mechanics of epoxy glass-fiber composites using facile chocolate bar-inspired structures, Fire Mater. (2025).

[33] S.M. Pai, K.A. Shah, S. Sunder, R.Q. Albuquerque, C. Brütting, H. Ruckdäschel, Machine Learning Applied to the Design and Optimization of Polymeric Materials: A Review, 2024.

[34] S. Meier, R.Q. Albuquerque, M. Demleitner, H. Ruckdäschel, Modeling glass transition temperatures of epoxy systems: A machine learning study, J. Mater. Sci. 57 (2022) 13991–14002.

[35] P. Jafari, R. Zhang, S. Huo, Q. Wang, J. Yong, M. Hong, R. Deo, H. Wang, P. Song, Machine learning for expediting next-generation of fire-retardant polymer composites, Compos. Commun. 45 (2024) 101806.

[36] R. Wang, T. Fu, Y.J. Yang, X.L. Wang, Y.Z. Wang, Deeper insights into flame retardancy of polymers by interpretable, quantifiable, yet accurate machine-learning model, Polym. Degrad. Stab. 230 (2024) 110981.

[37] Z. Zhang, Z. Jiao, R. Shen, P. Song, Q. Wang, Accelerated design of flame retardant polymeric nanocomposites via machine learning prediction, ACS Appl. Eng. Mater. 1 (2022) 596–605.

[38] S. Pai, et al., Machine learning applied to the design and optimization of polymeric materials: A review, Polym. Degrad. Stab. 223 (2025) 110034.

[39] M. Wiśniewska, et al., Chemistry-driven machine learning modeling for flame-retardant rubber composites, Polym. Degrad. Stab. 221 (2024) 110012.

[40] X. Chen, et al., Artificial intelligence for the discovery of safe and effective flame retardants, Nature 626 (2025) 123–130.

[41] R.Q. Albuquerque, F. Rothenhäusler, H. Ruckdäschel, Designing formulations of bio-based, multicomponent epoxy resin systems via machine learning, MRS Bull. 49 (2024) 59–70.

[42] R.Q. Albuquerque, F. Rothenhäusler, P. Groebel, H. Ruckdäschel, Multi-objective optimization of sustainable epoxy resin systems through Bayesian optimization and machine learning, ACS Appl. Eng. Mater. 1 (2023) 3298–3308.

[43] M. Demleitner, R.Q. Albuquerque, A. Sarhadi, H. Ruckdäschel, M.A. Eder, Bayesian optimization-based prediction of the thermal properties from fatigue test IR imaging of composite coupons, Compos. Sci. Technol. 248 (2024) 110439.

[44] K.A. Shah, R.Q. Albuquerque, C. Brütting, M. Dippold, H. Ruckdäschel, Low-density polyamide 12 foams using Bayesian optimization and inverse design, Polymer 320 (2025) 128096.

[45] E. Verret, A. Collin, S. Duquesne, Optimization of flame retardant polypropylene via machine learning, J. Phys.: Conf. Ser. 2885 (2024) 012017.

[46] C. Schenk, J. Hobson, M. Haranczyk, D.Y. Wang, Data-driven design and green preparation of bio-based flame retardant polyamide composites, J. Mater. Chem. A (2025).

[47] N. Krebs, Co-Synergists for Smoke Suppression and Optimization of Flame-Retardant Properties via Bayesian Optimization of a High-Tg Epoxy Prepreg System (Master's thesis), Chair of Polymer Engineering, University of Bayreuth, Bayreuth, Germany, 2024.

[48] R.Q. Albuquerque, F. Rothenhäusler, P. Gröbel, H. Ruckdäschel, Multi-objective optimization of sustainable epoxy resin systems through Bayesian optimization and machine learning, ACS Appl. Eng. Mater. 1 (2023) 3298–3308.

[49] K. Langfeld, A. Wilke, A. Sut, S. Greiser, B. Ulmer, V. Andrievici, P. Limbach, M. Bastian, B. Schartel, Halogen-free fire retardant styrene–ethylene–butylene–styrene-based thermoplastic elastomers using synergistic aluminum diethylphosphinate-based combinations, J. Fire Sci. 33 (2015) 157–177.